Journal of Crustacean Biology Advance Access published 4 January 2019

The Crustacean Society

Journal of Crustacean Biology

Journal of Crustacean Biology 39(3) 253–260, 2019. doi:10.1093/jcbiol/ruy086

Valve calcification in the evolutionary history of marine ostracodes (Ostracoda)

Tatsuhiko Yamaguchi

1528-3 Ohsone-otsu, Nankoku, 783-0005, Japan

Correspondence: T. Yamaguchi; email: aka.tyam.aguchi032018@gmail.com

(Received 2 November 2017; accepted 15 September 2018)

ABSTRACT

The calcification of the two valves of ostracodes in evolutionary history is poorly understood. Previous studies hypothesized that valve calcification has intensified with the development of a more complex hingement, independently of phylogeny. The degree of calcification in a valve is assessed qualitatively, based on the valve thickness. I assessed the degree of valve calcification in 145 single-valve marine specimens from 14 families and tested the hypothesis of a relationship between valve calcification, hingement type, and phylogeny, using phylogenetic generalized linear squares (PGLS). The calcification index (CI) was calculated as the ratio of a single valve mass to its volume. Nested models were used to explain the valve mass and CI using valve thickness, valve surface area, valve volume, and hingement type. The results of PGLS support the hypothesis that both the valve mass and CI evolved independently of both phylogeny and hingement type in the evolutionary history of ostracodes. The mass and degree of valve calcification evolved with the thickness and surface area of the calcified procuticle together.

Key Words: biomineralization, calcification index, calcified valve mass, hingement type

EIGHTEENTH INTERNATIONAL SYMPOSIUM ON OSTRACODA

INTRODUCTION

Crustaceans, including ostracodes, have exoskeletons biomineralized with calcium and chitin. The appearance and development of the exoskeleton in evolutionary history remain speculative and hypothetical (e.g., Luquet, 2012). Calcite biomineralization of the exoskeleton correlates not only with the environmental water chemistry and diet, but also with the regulation of cell calcium concentrations and ecdysis (e.g., Wheatly, 1999). Understanding the biomineralization of exoskeletons should significantly extend our understanding of the evolution and nature of crustaceans.

Ostracodes have heavily calcified exoskeletons. For example, 82.7% of the weight of *Chlamydotheca* is attributable to calcium carbonate (Sohn, 1958). Ostracodes have two valves made of low-magnesium calcite. The valves contact on the dorsal side and are connected by the hingement.

Valve calcification during evolutionary history is still poorly understood. Previous studies have ranked the degree of calcification as "weakly," "well," or "strongly" calcified when assessing calcification qualitatively based on valve thickness (e.g., Benson *et al.*, 1961; Athersuch *et al.*, 1989; Park & Ricketts, 2003). Some researchers consider that valve calcification is associated with the hingement type of the valve (Pokorný, 1957; Benson, 1966; Hinz, 1993). Complex hingement types (e.g., amphidont type) occur with thick valves (heavily calcified valves), whereas simple hingement types (e.g., adont type) occur with thin valves (lightly calcified valves). The hingement type is a key character defining ostracode families and genera (e.g., Horne *et al.*, 2002). Yamaguchi (2003) constructed a molecular phylogeny of cytheroidean ostracodes and a phylogenetic tree at the family level, and modeled the evolutionary trend in hingement types. The model showed that the complex hingement types were derived from the simple types. He suggested that the evolution of the hingement was associated with valve calcification. Yamada (2007) constructed an alternative classification of the hingement type by observing the cross-sections of hingements with organic ligaments. He discussed the divergence of the hingement type and inferred that small changes in valve calcification drove the development of complex hingements. If calcification is linked to the diversification of complex hingement types, ostracodes have strongly calcified and reinforced their exoskeletons since the Ordovician (Hinz-Schallreuter & Schallreuter, 1999). Although the hingement type is often linked to the phylogeny of ostracodes, valve calcification is not considered to have been influenced by phylogeny but to be affected by the environment (Yamaguchi, 2003; Yamada, 2007; Yamada & Keyser, 2010). No studies have so far used quantitative data to test the hypothesis that valve calcification and hingement coevolved.

The study aimed to determine the single valve masses and sizes of 14 ostracode families from marine sediments and discuss the coevolution of calcification and hingement. To assess valve calcification quantitatively, I defined and used the calcification index (*CI*) calculated by dividing the mass of a single valve by its volume based on the concept of human bone density. Only five previous studies have reported the valve weights of six benthic species (Kesling & Takagi, 1961; Kesling & Crafts, 1962; Herman & Heip, 1982; Roca & Wansard, 1997; Bridgwater *et al.*, 1999). The coevolution of traits has been assessed quantitatively with phylogenetic generalized linear squares (PGLS), a regression model based on phylogenic trees (e.g., Symonds & Blomberg, 2014).

MATERIALS AND METHODS

Materials

From 26 marine sediment samples, 145 adult single valves of ostracodes were obtained (Supplementary material Table S2). Seventeen Paleocene samples were from sediment cores at Integrated Ocean Drilling Site U1407, off Newfoundland, northwestern Atlantic (Norris *et al.*, 2014). Two Pliocene and Pleistocene samples were collected from outcrops in Japan. Seven Holocene samples were from sediment cores from bays, shelves, and shelf slopes around the Japanese islands.

The fossil specimens were cleaned according to the method of Qin *et al.* (2016) and sonicated with 2% $(NaPO_3)_6$ solution for 2 s in an ultrasonic bath at a frequency of 43 kHz. The Holocene specimens were soaked in 2% NaClO solution for 3 h to remove any organic matter. Sediment particles were removed from the valves with a fine brush.

The specimens were identified as belonging to four suborders, 14 families, 26 genera, and 47 species. The classification of suprageneric taxonomic ranks was according to Brandão *et al.* (2018). All families and genera were extant. In taxa other than Cytherellidae, all the adult specimens had developed calcified inner lamellae (e.g., Horne *et al.*, 2002). Adult cytherellid specimens, which lack inner lamellae, showed more rounded posterodorsal margins than the juveniles (Brandão, 2008; Okada *et al.*, 2008; Antonietto *et al.*, 2012).

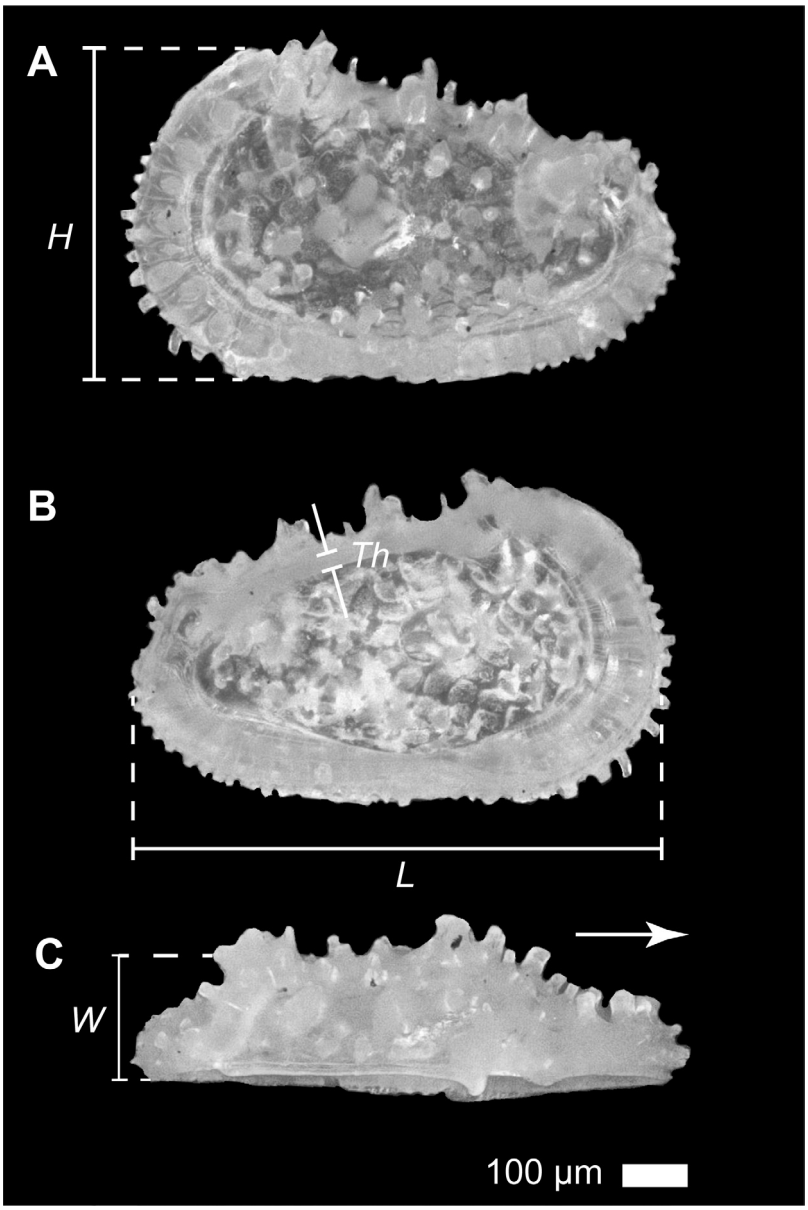

Figure 1. Measurements of a valve specimen. Light microscopic images of the adult left valve of *Acanthocythereis* sp. from sample NT14-04 PC02-01A, 1–3 cm. Lateral external (**A**), lateral internal (**B**), and dorsal (**C**) views. Arrow indicates the anterior direction; *L*, valve length; *H*, valve height; *W*, valve width; *Th*, valve thickness. Scale bar = 100 µm.

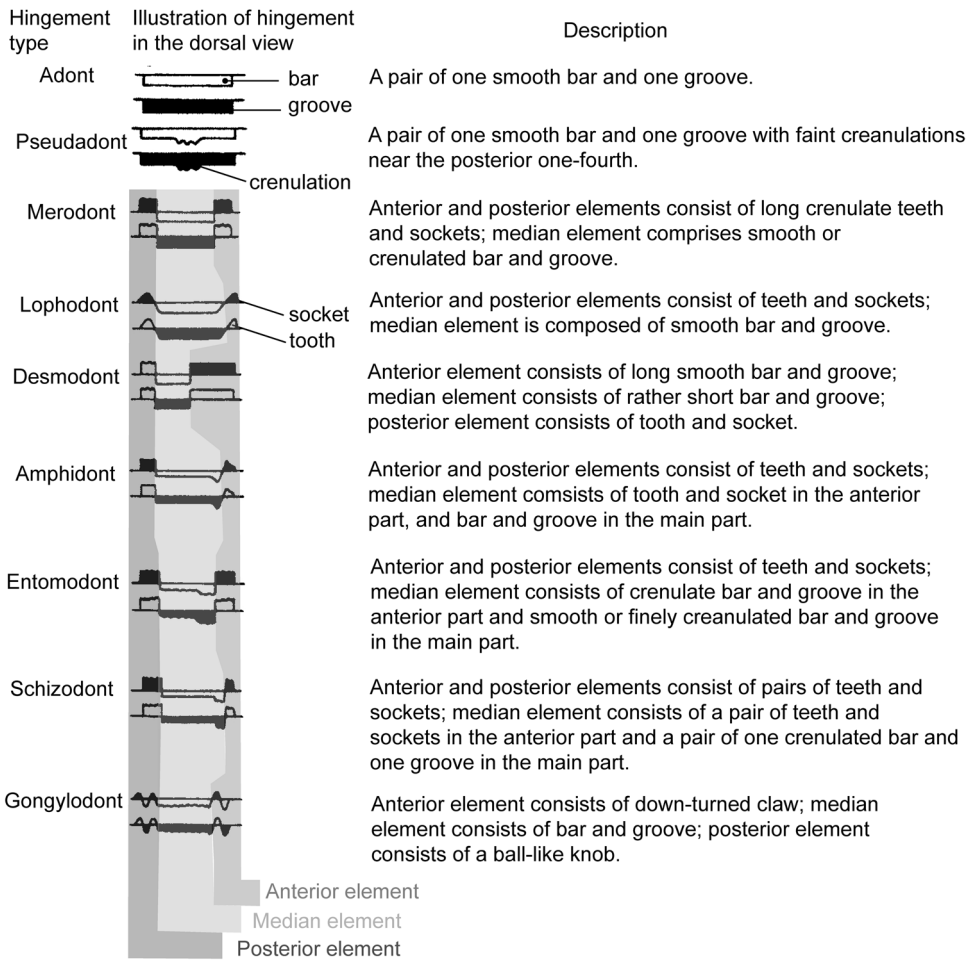

Figure 2. Hingement types (from Yamaguchi, 2003). The description is from Howe & Laurencich (1958) and Hanai (1961).

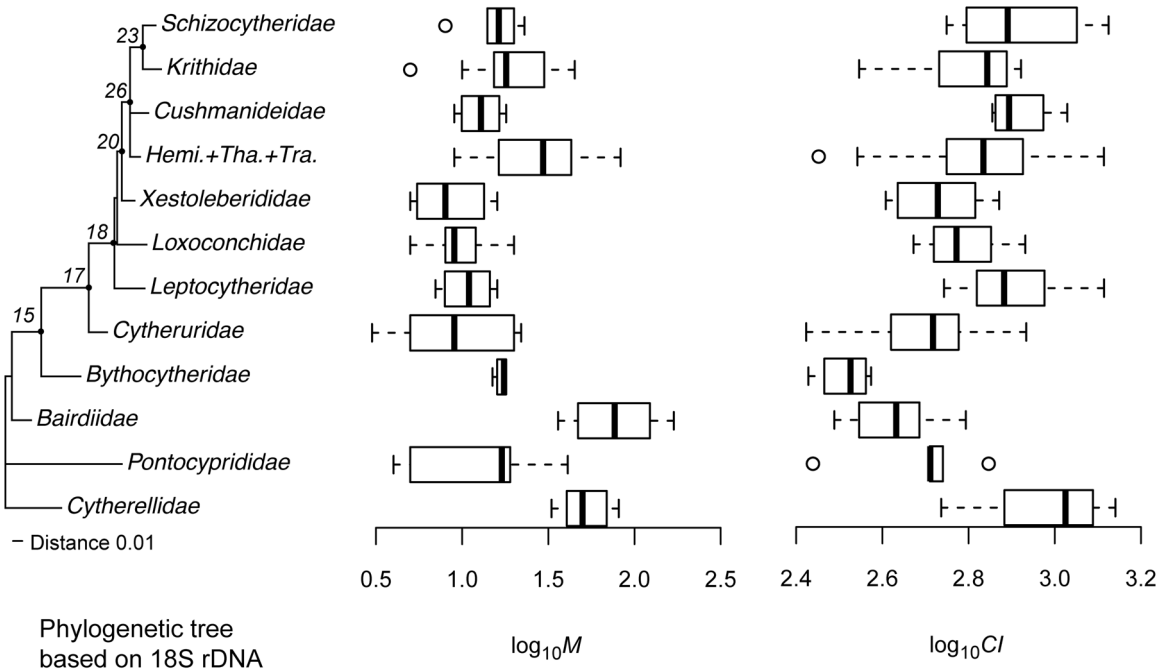

Figure 3. Phylogeny, $\log_{10}M$, and $\log_{10}CI$. The phylogenetic tree is modified from Tinn & Oakley (2008: Fig. 1), and was generated from an 18S rDNA dataset, using the maximum likelihood method. Circles indicate outliers. Numbers in italics at the nodes on the tree correspond to those of Tinn & Oakley (2008). "Hemi. + Tha. + Tra." indicates the Hemicytheridae–Thaerocytheridae–Trachyleberididae clade.

Measurement of valve size and valve thickness

I measured the length (*L*), height (*H*), and width (*W*) of the single valves at 300× magnification using a VHX-2000 digital microscope (Keyence, Osaka, Japan) (Supplementary material Table S3). The precision of the measurements was 0.645 µm at 1σ. The lengths of the spines and marginal denticles were excluded from the measurements (Fig. 1). The thickness changes in a single valve specimen when ostracode carapaces are observed in thin section (e.g., Scott, 1961). The hingement thickness was considered the typical value for valve thickness (*Th*) in this study. Hingement is a trait found in all ostracode taxa. Left and right valves attach at the hingement. The hingement thicknesses of both valves are equivalent, even when the valves have asymmetric shapes. Because the hingement appears at the margin of a valve in internal view, measuring its size is easy. I measured the thickness at the center of the middle element of the hingement in each valve specimen at 400× magnification using the digital microscope (Fig. 1). The precision (1σ) of the measurement was 0.567 µm. The digital microscope was sited at the Kochi Core Center (KCC)/Center for Advanced Marine Core Research, Kōchi University, Kōchi, Japan. Precision was estimated from 90 repeated measurements made with a Zeiss (Zeiss, Oberkochen, Germany) stage micrometer (length: 1 mm).

Calculation of volume and surface area of valves

The valve volume (*V*) was calculated under the assumption of semi-ellipsoid-shaped valves (Yasuhara *et al.*, 2016):

$$V = \frac{1}{2} \times \frac{4}{3} \times 3.14 \times \frac{L}{2} \times \frac{H}{2} \times W,$$

where *L*, *H*, and *W* are the valve length, valve height, and valve width, respectively.

Under this assumption, the approximate formula for the valve surface area (*SA*) is expressed as:

$$SA = \frac{1}{2} \times 4 \times 3.14 \times \sqrt[p]{\frac{\left\{\left(\frac{L}{2} \times \frac{H}{2}\right)^p + \left(\frac{L}{2} \times W\right)^p + \left(\frac{H}{2} \times W\right)^p\right\}}{3}},$$

where *p* is a constant of 1.60. The relative error is at most 1.178% (Cantrell, 2004). *SA* excludes the area of the intersection ellipse on the assumption that this area was not covered with a calcified layer. The assumption of a semi-ellipsoid shape will overestimate *V* in specimens with alae and underestimate *SA* in specimens with surface ornamentation.

Valve mass and calcification index

The specimens were weighed with a SC2 microbalance (Sartorius, Goettingen, Germany) at KCC (Supplementary material Table S2). The precision (1σ) was 0.607 µg, which was estimated from 14 repeated measurements of five defined specimens. Like human bone density and the *CI* of gastropods (Graus, 1974), *CI* (µg mm^{-3}) was defined as:

$$CI = \frac{M}{V},$$

where *M* and *V* are the valve mass and volume, respectively.

Hingement type

The division of the hingement types at the family level was according to Hinz-Schallreuter & Schallreuter (1999) (Fig. 2). To incorporate the hingement type into the regression models, the nine hingement types were coded as follows: 1 = adont type; 2 = lophodont type; 3 = merodont type; 4 = entomodont type; 5 = gongylodont type; 6 = amphidont type; 7 = desmodont type; 8 = pseudadonta type; and 9 = schizodont type.

Phylogeny

The molecular phylogenetic tree of Tinn & Oakley (2008) was used for the PGLS analysis (Fig. 3). It was based on the Ostracoda 18S rDNA sequences available in GenBank and generated with the maximum likelihood (ML) method (Tinn & Oakley, 2008). I selected specific nodes and leaves, and modified the original phylogenetic tree. The analyses of Yamaguchi (2003) and Tinn & Oakley (2008) indicated that the family Trachyleberididae is paraphyletic. Because datasets for PGLS assume that all taxa are monophyletic (Garland *et al.*, 1999), I grouped the families Hemicytheridae, Thaerocytheridae, and Trachyleberididae into a single clade. The modified phylogenetic tree showed 12 lineages at the family level.

Phylogenetic generalized linear squares (PGLS)

PGLS was performed with ML and restricted ML (REML) approaches. The ML approach is even applicable to models with small sample sizes (Kamilar & Cooper, 2013) and REML is an

Table 1. Hingement type and mean for valve size (*Th*, valve thickness; *SA*, surface area of a single valve; *V*, volume of a single valve), mass of a single valve (*M*), and calcification index (*CI*) in ostracode clades; *N*, number of specimens.

Clade	Hingement type	*Th* (mm)	*SA* (mm^2)	*V* (mm^3)	*M* (µg)	*CI* (µg mm^{-3})	*N*
Cytherellidae	adont	0.022	0.58	0.056	54	1017	16
Pontocyprididae	adont	0.014	0.41	0.03	17	511	5
Bairdiidae	adont	0.021	1.29	0.18	84	439	14
Bythocytheridae	lophodont	0.012	0.58	0.052	17	329	4
Cytheruridae	merodont	0.014	0.3	0.023	12	519	13
Leptocytheridae	entomodont	0.012	0.24	0.014	11	809	12
Loxoconchidae	gongylodont	0.014	0.26	0.017	11	628	9
Xestoleberididae	merodont	0.012	0.26	0.017	9	552	11
Hemicytheridae + Thaerocytheridae + Trachyleberididae	amphidont	0.018	0.51	0.048	31	722	36
Cushmanideidae	desmodont	0.012	0.27	0.016	13	839	4
Krithidae	pseudadont	0.016	0.43	0.035	22	647	15
Schizocytheridae	schizodont	0.014	0.29	0.019	16	866	6

alternative to ML that focuses on the estimation of the variance components because the variance components calculated with M are biased when the samples are small. The REML estimates for small samples are more nearly unbiased. I considered *Th*, *SA*, *V*, and hingement type as the predictor variables to explain the geometric mean of *M*, whereas I assume *Th*, *SA*, and hingement type as the variables to explain the geometric mean of *CI* and to identify candidate models. The analysis requires a knowledge of the phylogenetic relationships to produce an estimate of the expected covariance in the cross-species data. PGLS uses phylogenetic signals, which are defined as the tendency for related species to resemble each other more than they resemble species selected randomly from a phylogenetic tree (Blomberg & Garland, 2002; Blomberg *et al.*, 2003; Revell *et al.*, 2008). Pagel's λ was used as the index of phylogenetic signal. Pagel's λ varies continuously from zero to one (Pagel, 1997, 1999). λ = 0 means no phylogenetic signal in the trait, indicating that the trait evolved independently of phylogeny and that closely related taxa are not more similar, on average, than distantly related taxa and λ = 1 means a strong phylogenetic signal, indicating that the trait has evolved according to the Brownian motion model of evolution. Values intermediate between 0 and 1 indicate that although there is a phylogenetic signal in the trait, it evolved according to a process other than pure Brownian motion.

The ML and REML estimates of λ and the ML estimate of the corrected Akaike information criterion (AICc) were calculated. AICc is defined as (Sugiura, 1978):

$$AICc = -2\ln Lik + \frac{2kn}{(n-k-1)},$$

where *k*, *n*, and *Lik* are the number of parameters, the number of samples, and the maximized value of the likelihood function of the model, respectively. I also estimated the adjusted R^2 in each model regression. The ML and REML estimations calculated the coefficients and probability values of the intercept and the predictor variables using the software R (R Core Team, 2017) and the *caper* package (Orme *et al.*, 2013). In the ML approach, competing models with lower AICc values are deemed to be the best approximating model. I calculated the difference between the lowest AICc value and the AICc value for each model, ΔAICc. Models with ΔAICc < 2 were selected as the "best-fitted" models (Burnham & Anderson, 2002). The model candidates included models that were calculated using ordinary least squares (OLS). The relative strength of each model was determined as the Akaike weight using the model averaging method. The Akaike weight can be considered analogous to the probability that a given model is the best-approximating model. Summing the weights of the models in which the variable appeared, I estimated the relative importance of each predictor variable. I also calculated the weighted averages (coefficients) of the predictor variable estimates and their 95% confidence intervals. I averaged the models using the R software package "MuMIn" (Bartoń, 2018). The R packages "ape" (Paradis *et al.*, 2004) and "phytools" (Revell, 2012) were also used.

RESULTS

The value of *M* ranged between 3 and 169 μg (median 19 μg), and *CI* ranged between 1,300 and 3,6022 μg mm^{-3}, with a median of 16,245 μg mm^{-3}. The Kolmogorov–Smirnov two-sided test failed to reject the hypothesis that $\log_{10}M$ and $\log_{10}CI$ were not normally distributed ($\log_{10}M$: D = 0.069, *P* = 0.50; $\log_{10}CI$: D = 0.049, *P* = 0.87). I therefore regarded the distributions of $\log_{10}M$ and $\log_{10}CI$ as normal (Supplementary material Fig. S1). In the median, Xestoleeberididae and Bairdiidae had the lowest and the highest $\log_{10}M$, respectively. Bythocytheridae had the lowest $\log_{10}CI$, and Cytherellidae had the highest $\log_{10}CI$ (Fig. 3, Table 1). The result indicates variety of the mass and degree of the calcification, as previously recognized (e.g., Benson *et al.*, 1961).

When the ML and OLS approaches were used, ΔAICc < 2 selected two PGLS models for $\log_{10}M$ with the predictor variables *Th*, *SA*, and *V* from 30 candidate models (Table 2 and Supplementary material Table S4). Considering the coefficients of the intercepts and all the predictor variables, the model is preferred by ΔAICc and the intercept and predictor variables with significance (*P* < 0.05) (Table 3 and Supplementary material Table S5). Model averaging indicated that the parameter weight of *Th* was the greatest among all four predictor variables (Table 4). Only the 95% confidence interval of the coefficient of *Th* did not contain zero. Therefore, the model with predictor variables for both *Th* and *SA* was selected as the best-fitting model for $\log_{10}M$ from the 30

Table 2. Best approaching models (ΔAICc < 2) predicting $\log_{10}M$ in marine ostracodes, calculated with PGLS; REML, restricted maximum likelihood; ML, maximum likelihood; AICc, corrected Akaike information criterion; Wi, Akaike weight; *Th*, valve thickness; *SA*, surface area of a single valve; *V*, volume of a single valve.

Model components	λ (REML)	λ (ML)	ΔAICc	W_i	Adjusted R^2
Th + *SA*	0	0	0	0.448	0.972
Th + *SA* + *V*	0	0	0.404	0.366	0.978

Table 4. Coefficients, their 95% confidence intervals, and the relative importance of the predictor variables of $\log_{10}M$.

Predictor variable	Coefficient	95% confidence interval	Relative importance
Th	51.56	(37.87, 65.25)	1
SA	0.85	(-0.26, 1.95)	0.99
V	-5.15	(-10.76, 0.46)	0.48
Hingement	0.01	(-0.0073, 0.028)	0.18

Table 5. Best approaching models (ΔAICc <2) predicting $\log_{10}CI$ in marine ostracodes, calculated with PGLS.

Model components	λ (REML)	λ (ML)	ΔAICc	W_i	Adjusted R^2
Th + *SA*	0	0	0	0.515	0.699
Th + *SA* + *Hingement*	0.992	0	1.366	0.26	0.744

Table 3. Maximum likelihood (ML) and restricted maximum likelihood (REML) estimates of coefficients and probability (*P*) for the predictor variables of $\log_{10}M$.

Model components	Intercept		*Th*		*SA*		*V*	
	Coefficient	*P*	Coefficient	*P*	Coefficient	*P*	Coefficient	*P*
Th + *SA*	0.304725811	0.0079	52.88855322	3.30×10^{-5}	0.408217661	2.0×10^{-4}	-	-
Th + *SA* + *V*	0.174645309	0.14	49.78288268	5.30×10^{-5}	1.267087296	2.6×10^{-2}	–0.553712988	0.1

Table 6. Maximum likelihood (ML) and restricted maximum likelihood (REML) estimates of the coefficients and probability (*P*) for the predictor variables of $\log_{10}CI$.

Model components	Intercept		*Th*		*SA*		*Hingement*	
	Coefficient	*P*	Coefficient	*P*	Coefficient	*P*	Coefficient	*P*
Th + *SA*	1.442015	8.8×10^{-7}	40.695322	2.0×10^{-3}	–0.481760	5.5×10^{-4}	-	-
Th + *SA* + *Hingement*	1.319676	1.18×10^{-5}	42.714049	1.3×10^{-3}	–0.430024	1.5×10^{-3}	0.018206	0.15

Table 7. Coefficients, their 95% confidence intervals, and the relative importance of the predictor variables of $\log_{10}CI$.

Predictor variable	Coefficient	95% confidence interval	Relative importance
Th	39.82	(16.52, 63.13)	0.82
SA	–0.44	(–0.69, –0.19)	0.8
Hingement	0.022	(–0.0075, 0.051)	0.36

candidate models (Table 2 and Supplementary material Table S4). The best-fitting model indicates λ was 0 (Table 2). ΔAICc < 2 chooses two PGLS models for $\log_{10}CI$ with *Th*, *SA*, and the hingement parameters (Table 5 and Supplementary material Table S6). Both the *Th* and *SA* parameters were significant ($P < 0.05$) in both the two models, but the hingement parameter was not (Table 6 and Supplementary material Table S7). The model for $\log_{10}CI$ is favored by the low ΔAICc with significant intercept and predictor variable ($P < 0.05$) from the 16 candidate models. Model averaging indicated that both *Th* and *SA* were highly relatively important (Table 7), because the 95% confidence intervals of their coefficients did not contain zero. The model with predictor variables for both *Th* and *SA* was thus selected as the best-fit model for $\log_{10}CI$. The best-fitting model indicates λ was 0 (Table 5).

DISCUSSION

The best-fitted models for $\log_{10}M$ and $\log_{10}CI$ showed Pagel's λ = 0 (Tables 2, 5), indicating that the calcified mass and the calcification of the valves evolved independently of the ostracode phylogeny and that closely related taxa are not more similar, on average, than distantly related taxa. These results support the previous hypothesis (Yamaguchi, 2003; Yamada, 2007) that valve calcification has not been influenced by phylogeny. Considering the relationship between the phylogenetic signal and the evolutionary process (e.g., Blomberg *et al.*, 2003; Revell *et al.*, 2008), the low phylogenetic signal suggests that the valve calcification may either be hardly changed on the time scale of phylogeny or be extremely changeable.

The results of this study do not support the contention that the hingement type has influenced the mass and degree of calcification of single valves. The best-fitted models for both $\log_{10}M$ and $\log_{10}CI$ did not include a predictor variable for hingement. In the model averaging results, hingement had the lowest relative importance (Tables 4, 7), and the 95% confidence interval for the coefficient of hingement included zero. The hingement type cannot therefore be considered to significantly explain $\log_{10}M$ or $\log_{10}CI$. This quantitative analysis thus fails to support the conclusion of previous studies that valve calcification is associated with hingement type (Pokorný, 1957; Benson, 1966; Hinz-Schallreuter & Schallreuter, 1999; Yamaguchi, 2003; Yamada, 2007). Ostracodes have not reinforced their exoskeleton throughout evolutionary history in parallel with the diversification of the complex hingement types.

The PGLS results indicate that the mass and density of the calcified procuticle are dependent on the procuticle surface area and thickness. Predictor variables of the best-fitted models were *Th* and *SA*, which reflect thickness and surface area of the calcified valve (procuticle), respectively. When Keyser & Walter (2004) observed the cell layers beneath the outer lamella and analyzed their chemical composition, they found that calcium phosphate granules are stored in the epidermal cells before ecdysis and the granules penetrate the uncalcified procuticle. The granules are then portioned and altered to tiny granules of amorphous calcium carbonate. The amorphous carbonate granules are transformed into calcite during procuticle calcification after ecdysis. The concentrations of both amorphous calcium carbonate and calcium phosphate granules in the uncalcified procuticle correlate with the density of the calcified procuticle. This study indicates that both the thickness and the surface area of the procuticle have evolved with the mass and density of the calcified procuticle. A thicker calcified procuticle increases growths of the mass and density of the calcified procuticle, whereas a smaller surface area of the procuticle increases growth of the density of the calcified procuticle (Tables 3, 6). Aladin & Potts (1996) observed differences in the cell and cuticle morphologies under high- and low-salinity conditions. Previous studies had noted that the environmental parameters of the ostracode habitat (such as water temperature, salinity, and calcium concentrations in water) affect carapace calcification (Roca & Wansard, 1997; Mezquita *et al.*, 1999; Yamada & Keyser, 2010; Decrouy *et al.*, 2011a, b). The mass and density of the calcified procuticle are thus possibly affected by environmental parameters, including water chemistry and diets, and are physiological responses to the environment.

SUPPLEMENTARY MATERIAL

Supplementary material is available at *Journal of Crustacean Biology* online.

S1 Figure. Histograms of $\log_{10}M$ and $\log_{10}CI$.

S2 Table. Materials and their sampling localities.

S3 Table. Valve weight and size measurements of marine ostracode taxa.

S4 Table. All candidate models of $\log_{10}M$.

S5 Table. OLS and PGLS (ML and REML estimates) of the coefficients and probability values (*P*) of the predictor variables of $\log_{10}M$ in all candidate models.

S6 Table. All candidate models of $\log_{10}CI$.

S7 Table. OLS and PGLS (ML and REML estimates) of the coefficients and probability values (*P*) of the predictor variables of $\log_{10}CI$ in all candidate models.

ACKNOWLEDGMENTS

The ostracode specimens used in this study were from sediment samples provided by the Integrated Ocean Drilling Program and from Holocene sediment core samples provided by the Japan Agency for Marine-Earth Science and Technology. I am grateful to A. Matsuki, K. Shimizu, and T. Yabuki for assistance with collecting sediment samples; to T. Matsuzaki for help in using the digital microscope; and to D. Horne, A. Lord, and L. Antonietto for their suggestion about the morphological features of adult Cytherellidae

in the OSTRACON mailing list. This study was financially supported by JSPS KAKENHI (grants JP16K05590 and JP18H03364) of the Japan Society of Promotion of Science. I thank T. Oakley and an anonymous reviewer for their critical reviews and constructive suggestions. Also I thank P. Castro for his suggestions and editing the manuscript. This study was undertaken during my tenure at the Center for Advanced Marine Core Research, Kochi University.

REFERENCES

Aladin, N.V. & Potts, W.T.W. 1996. The osmoregulatory capacity of the Ostracoda. *Journal of Comparative Physiology B*, **166**: 215–222.

Antonietto, L., Machado, C.P., Do Carmo, D.A. & Rosa, J.W.C. 2012. Recent Ostracoda (Arthropoda, Crustacea) from São Pedro-São Paulo Archipelago, Brazil: a preliminary approach. *Zootaxa*, **3335**: 29–53.

Athersuch, J., Horne, D.J. & Whittaker, J.E. 1989. *Marine and brackish water ostracods (superfamilies Cypridacea and Cytheracea): Key and notes for the identification of the species*. The Linnean Society of London and the Estuarine and Brackish-water Sciences Association, Avon, UK.

Bartoń, K. 2018. *MuMIn: Multi-Model Inference. R package version 1.40.4* [https://CRAN.R-project.org/package=MuMIn].

Benson, R.H. 1966. Recent marine podocopid ostracodes. *Oceanography and Marine Biology: An Annual Review*, **4**: 213–232.

Benson, R.H., Berdan, J.M., Bold, W.A. Van den, Hanai, T., Hessland, I., Howe, H.V., Kesling, R.V., Levinson, S.A., Reyment, R.A., Moore, R.C., Scott, H.W., Shaver, R.H., Sohn, I.G., Stover, L.E., Swain, F.M. & Sylvester-Bradley, P.C. 1961. Systematic descriptions. In: *Treatise on invertebrate paleontology, Part Q, Artheropoda 3* (R.C. Moore, ed.) pp. Q99–Q421. Geological Society of America & University of Kansas Press, New York.

Blomberg, S.P. & Garland, T.J. 2002. Tempo and mode in evolution: phylogenetic inertia, adaptation and comparative methods. *Journal of Evolutionary Biology*, **15**: 899–910.

Blomberg, S.P., Garland, T.J. & Ives, A.R. 2003. Testing for phylogenetic signal in comparative data: Behavioral traits are more labile. *Evolution*, **57**: 717–745.

Brandão, S.N. 2008. First record of a living Platycopida (Crustacea, Ostracoda) from Antarctic water and a discussion on *Cytherella serratula* (Brady, 1880). *Zootaxa*, **1866**: 349–372.

Brandão, S.N., Angel, M.V., Karanovic, I., Perrier, V. & Yasuhara, M. 2018. World Ostracoda Database [http://www.marinespecies.org/ostracoda].

Bridgwater, N.D., Holmes, J.A. & O'Hara, S.L. 1999. Complex controls on the trace-element chemistry of non-marine ostracods: an example from Lake Pátzcuaro, central Mexico. *Palaeogeography, Palaeoclimatology, Palaeoecology*, **148**: 117–131.

Burnham, K.P. & Anderson, D.R. 2002. *Model selection and multimodel inference*, Edn. 2. Springer, New York.

Cantrell, D.W. 2004. Surface area of an ellipsoid[https://web.archive.org/web/20110930084035/http://www.numericana.com/answer/ellipsoid.htm].

Decrouy, L., Vennemann, T.W. & Ariztegui, D. 2011a. Controls on ostracod valve geochemistry: Part 1. Variations of environmental parameters in ostracod (micro-)habitats. *Geochimica et Cosmochimica Acta*, **75**: 7364–7379.

Decrouy, L., Vennemann, T.W. & Ariztegui, D. 2011b. Controls on ostracod valve geochemistry: Part 2. Carbon and oxygen isotope compositions. *Geochimica et Cosmochimica Acta*, **75**: 7380–7399.

Garland, T.J., Midford, P.E. & Ives, A.R. 1999. An introduction to phylogenetically based statistical methods, with a new method for confidence intervals on ancestral values. *American Zoologist*, **39**: 374–388.

Graus, R.R. 1974. Latitudinal trends in the shell characteristics of marine gastropods. *Lethaia*, **7**: 303–314.

Hanai, T. 1961. Studies on the Ostracoda from Japan: hingement. *Journal of the Faculty of Science, University of Tokyo*, **13**: 345–377.

Herman, P. & Heip, C. 1982. Growth and respiration of *Cyprideis torosa* Jones 1850 (Crustacea Ostracoda). *Oecologia*, **54**: 300–303.

Hinz, I.C.U. 1993. Evolutionary trends in archaeocopid ostracods. In: *Ostracoda in the earth and life sciences* (K.G. McKenzie & P.J. Jones, eds.), pp. 3–12. A.A. Balkema, Rotterdam, The Netherlands.

Hinz-Schallreuter, I. & Schallreuter, R. 1999. *Ostrakoden*. Ferdinand Enke Verlag, Stuttgart, Germany.

Horne, D.J., Cohen, A. & Martens, K. 2002. Taxonomy, morphology and biology of Quaternary and living Ostracoda. In: *The Ostracoda: Applications in Quaternary research* (J.A. Holmes & A.R. Chivas, eds.), pp. 5–36. American Geophysical Union, Washington D.C., USA.

Howe, H.V. & Laurencich, L. 1958. *Introduction of the study of Cretaceous Ostracoda*. Louisiana State University Press, Baton Rouge, LA, USA.

Kamilar, J.M. & Cooper, N. 2013. Phylogenetic signal in primate behaviour ecology and life history. *Philosophical Transactions of the Royal Society B*, **368**: 20120341 [doi: 10.1098/rstb.2012.0341].

Kesling, R.V. & Crafts, F.C. 1962. Ontogenetic increase in Archimedean weight of the ostracod *Chlamydotheca unispinosa* (Baird). *American Midland Naturalist*, **68**: 149–153.

Kesling, R.V. & Takagi, R.S. 1961. Evaluation of Przibram's law for ostracods by use of the Zeuthen Cartesian-Diver weighing technique. *Contributions from the Museum of Paleontology, University of Michigan*, **17**: 1–58.

Keyser, D. & Walter, R. 2004. Calcification in ostracodes. *Revista Española de Micropaleontología*, **36**: 1–11.

Luquet, G. 2012. Biomineralizations: insights and prospects from crustaceans. *Zookeys*, **176**: 103–121.

Mezquita, F., Roca, J.R. & Wansard, G. 1999. Moulting, survival and calcification: the effects of temperature and water chemistry on an ostracod crustacean (*Herpetocypris intermedia*) under experimental conditions. *Archiv für Hydrobiologie*, **146**: 219–238.

Norris, R.D., Wilson, P.A., Blum, P. & the Expedition 342 scientists. 2014. Paleogene Newfoundland sediment drifts and MDHDS Test. *Proceedings of the Integrated Ocean Drilling Program*, **342** [doi: 10.2204/iodp.proc.342.2014].

Okada, R., Tsukagoshi, A., Smith, R.J. & Horne, D.J. 2008. The ontogeny of the platycopid *Keijcyoidea infralittoralis* (Ostracoda: Podocopa). *Zoological Journal of the Linnean Society*, **153**: 213–237.

Orme, D., Freckleton, R., Thomas, G., Petzoldt, T., Fritz, S., Isaac, N. & Pearse, W. 2013. *caper: Comparative Analyses of Phylogenetics and Evolution in R. R package version 0.5.2*. [https://CRAN.R-project.org/package=caper].

Pagel, M. 1997. Inferring evolutionary process from phylogenies. *Zoologica Scripta*, **26**: 331–348.

Pagel, M. 1999. Inferring the historical patterns of biological evolution. *Nature*, **401**: 877–884.

Paradis, E., Claude, J. & Strimmer, K. 2004. APE: Analyses of Phylogenetics and Evolution in R language. *Bioinformatics*, **20**: 289–290.

Park, L.E. & Ricketts, R.D. 2003. Evolutionary history of the Ostracoda and the origin of nonmarine faunas. In: *Bridging the gap: Trends in the Ostracode biological and geological sciences. The Paleontological Society Papers*, Vol. 9 (L.E. Park & A.J. Smith, eds.), pp. 11–35. The Paleontological Society, New Haven, CT, USA.

Pokorný, V. 1957. The phylomorphogeny of the hinge in Podocopida (Ostracoda, Crustacea) and its bearing on the taxonomy. *Acta Universitatis Carolinae, Geologica*, **1957**: 1–22.

Qin, B., Li, T., Xiong, Z., Algeo, T.J. & Chang, F. 2016. An improved protocol for cleaning of planktonic Foraminifera for shell weight measurement. *Journal of Sedimentary Research*, **86**: 431–437.

R Core Team, 2017. *R: A language and environment for statistical computing*. R Foundation for Statistical Computing, Vienna, Austria [https://www.R-project.org/].

Revell, L.J. 2012. phytools: An R package for phylogenetic comparative biology (and other things). *Methods in Ecology and Evolution*, **3**: 217–223.

Revell, L.J., Harmon, L.J., Collar, D.C. & Oakley, T. 2008. Phylogenetic signal, evolutionary process, and rate. *Systematic Biology*, **57**: 591–601.

Roca, J.R. & Wansard, G. 1997. Temperature influence on development and calcification of *Herpetocypris brevicaudata* Kaufmann, 1900 (Crustacea: Ostracoda) under experimental conditions. *Hydrobiologia*, **347**: 91–95.

Scott, H.W. 1961. Shell morphology of Ostracoda. In: *Treatise on invertebrate palaeontology*, Part Q Arthropoda 3 (R.C. Moore, ed.), pp. Q21–Q37. University of Kansas Press, Lawrence, KS, USA.

Sohn, I.G. 1958. Chemical constituents of ostracodes; some applications to paleontology and paleoecology. *Journal of Paleontology*, **4**: 730–736.

Sugiura, N. 1978. Further analysis of the data by Akaike' S information criterion and the finite corrections. *Communications in Statistics—Theory and Methods*, **7**: 13–26.

Symonds, M.R.E. & Blomberg, S.P. 2014. A primer on phylogenetic generalised least squares. In: *Modern phylogenetic comparative methods and their application in evolutionary biology* (L.Z. Garamszegi, ed.), pp. 105–130. Springer-Verlag, Berlin & Heidelberg, Germany.

Tinn, O. & Oakley, T.H. 2008. Erratic rates of molecular evolution and incongruence of fossil and molecular divergence time estimates in Ostracoda (Crustacea). *Molecular Phylogenetics and Evolution*, **48**: 157–167.

Yamada, S. 2007. Structure and evolution of podocopan ostracod hinges. *Biological Journal of the Linnean Society*, **92**: 41–62.

Yamada, S. & Keyser, D. 2010. Calcification of the marginal infold in podocopid ostracods. *Hydrobiologia*, **638**: 213–222.

Yamaguchi, S. 2003. Morphological evolution of cytherocopine ostracods inferred from 18S ribosomal DNA sequences. *Journal of Crustacean Biology*, **23**: 131–153.

Yasuhara, M., Doi, H., Wei, C.-L., Danovaro, R. & Myhre, S.E. 2016. Biodiversity–ecosystem functioning relationships in long-term time series and palaeoecological records: deep sea as a test bed. *Philosophical Transactions of the Royal Society B: Biological Sciences*, **371**: 20150282 [doi:10.1098/rstb.2015.0282].

Wheatly, M.G. 1999. Calcium homeostasis in Crustacea: the evolving role of branchial, renal, digestive and hypodermal epithelia. *Journal of Experimental Zoology*, **283**: 620–640.